A 915 MHz Wristwatch-Integrated Antenna for Wireless Health Monitoring

Sanjeev Kumar[1], John L. Buckley[1], John Barton[1], Robert Newberry[2], Gary Dunlop[2], Matthew Rodencal[2], Carlo Webster[1], Melusine Pigeon[1], William G. Scanlon[1], Brendan O'Flynn[1]
[1]Tyndall National Institute, University College Cork, Cork, Ireland, sanjeev.kumar@tyndall.ie
[2]Sanmina Corporation, 13000 S. Memorial Parkway, Huntsville, AL 35803, USA

***Abstract*—A compact 915 MHz antenna integrated within a wristwatch wireless sensor device is presented. The antenna is a variant of a planar inverted-F antenna (PIFA) and uses a dual-resonator configuration. The results of simulation and measurement are shown to be in good agreement with the antenna exhibiting desirable impedance and radiation characteristics together with low Specific Absorption Rate (SAR) performance. The antenna is fabricated using a low cost flexible printed circuit and is fully integrated into the watch device. Measurements on the prototype antenna show a −10 dB impedance bandwidth of 30 MHz, a peak realized gain of −4.9 dBi and a peak radiation efficiency of 15.9% at 915 MHz. The antenna also has a low SAR value of 0.003 W/kg making it suitable for a wide range of wrist-worn wireless applications.**

***Index Terms*—antenna, wearable, Sub-GHz, wristwatch-integration, PIFA, clinical-trials.**

I. Introduction

With the rapid development of wireless sensor network (WSN) and internet of things (IoT) technology, there is a growing demand for wrist-worn smart devices because of its widespread applications in sports, security, fitness tracking and healthcare [1]. Currently, the majority of wristwatch antennas are designed to operate using the IEEE 802.11 standard 2.4 GHz frequency band [2]. However, the 2.4 GHz band has issues such as overcrowding because of its widespread use in Wi-Fi, Bluetooth, ZigBee etc. [3]. This overcrowding causes mutual interference and data packet collision and leads to network disruption [3]. The Sub-GHz industrial scientific and medical (ISM) band can offer potential advantages over conventional 2.4 GHz band such as reduced free-space path loss, reduced band congestion and the potential to use lower power and lower cost radio transceivers [4]. However, the design of antennas for these Sub-GHz frequencies is also challenging due to size constraints.

In recent years, a number of smartwatch antennas operating at the Sub-GHz band has been proposed in the literature. In [5], a dual-band wearable loop antenna using a metallic wristwatch frame is reported. In the Sub-GHz band, this antenna has a -10 dB impedance bandwidth of 180 MHz; however, it has a radiation efficiency of less than 7%. In further work, a dipole and two types of monopole antennas operating in the 700 MHz to 2.7 GHz frequency band are presented in [6]. The dipole antenna has a wide impedance bandwidth of 160 MHz in the 900 MHz band. However, this antenna has a low radiation efficiency of 6.3% at 900 MHz. A low profile helical 868 MHz wristband antenna for radio frequency identification (RFID) is reported in [7]. The achieved -10 dB impedance bandwidth of this antenna is 17 MHz but has a low peak realized gain of -13 dBi at 868 MHz. In [8], the authors present a wristwatch planar inverted-F antenna (PIFA), where the on-body measured results show a -10 dB impedance bandwidth of 26.4 MHz, a peak realized gain of -0.57 dBi and a radiation efficiency of 46.8% at 915 MHz. However, when compared with the literature, the height of this antenna from the nearest ground plane is comparatively large (10.3 mm). In [4], the authors present a 915 MHz band meandered PIFA wristwatch antenna. This antenna has an on-body peak realized gain of -6.1 dBi, and a -10 dB impedance bandwidth of 55 MHz using an impedance matching network.

The focus of this work is to develop a compact, low-cost 915 MHz antenna that can be fully integrated within a limited space in a wristwatch device, with all surrounding electronics also in place. The developed antenna simultaneously achieves good impedance and radiation characteristics when compared against the state-of-the-art wrist-worn antennas and does not require an impedance matching network. The remainder of the paper is organised as follows. The antenna configuration of the proposed antennas is described in Section II. In Section III, the results obtained from antenna simulations and parametric analysis are discussed in detail. Antenna measurements are presented and discussed in Section IV. Finally, Section V presents the main conclusions of this work.

II. Antenna Design

The geometry of the proposed antenna is shown in Fig. 1. The antenna is a variant of a PIFA topology and is fed with an unbalanced feed with a signal at point *S* and ground at point *G*. The PIFA is comprised of two resonator arms denoted R_1 and R_2. The section between points *S* and *G* implement a shunt inductive element that is used to balance the large capacitance of arms R_1 and R_2 that are in close proximity to ground planes of the radio and sensor board beneath. The radio board feeds the antenna via spring contacts as shown in Fig. 1. The motherboard and sensor are responsible for measuring the heart rate and blood oxygen levels but are not discussed in detail in this work. The antenna is printed on a low-cost, 0.11 mm thick printed circuit with a polyimide substrate. The polyimide dielectric has a relative permittivity of ϵ_r = 3.1 and a loss tangent of $tan\delta$ = 0.0245 at 915 MHz. The dielectric

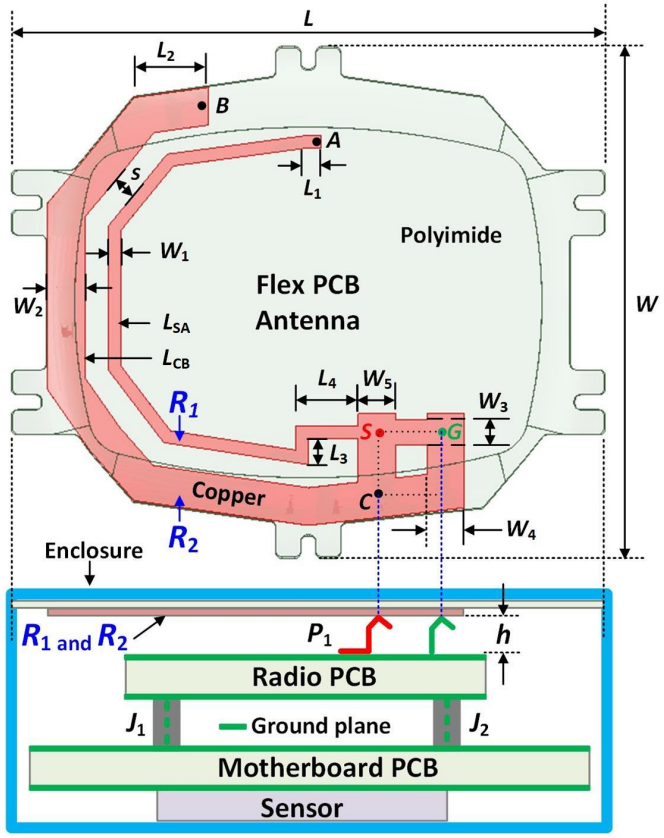

Fig. 1. Configuration of the antenna within the smartwatch device; L = 48, W = 41, L_{SA} = 54, L_{CB} = 58, L_1 = 1, L_2 = 6, L_3 = 2, L_4 = 5, W_1 = 1, W_2 = 3, W_3 = 2, W_4 = 3, W_5 = 3, s = 2; Unit: mm.

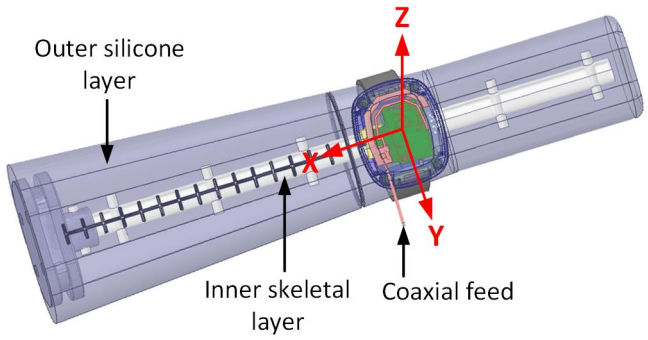

Fig. 2. Wristwatch model placed on the a Speag phantom arm [14].

properties of all the materials were derived from measurements using a dielectric assessment kit (DAK) from Speag [13].

Fig. 2 shows the EM simulation model. The antenna is integrated within the wristwatch device as shown. The wristwatch enclosure uses an acrylonitrile styrene acrylate (ASA) material with a measured ϵ_r = 2.9 and $tan\delta$ = 0.033 at 915 MHz. The maximum dimension of the wristwatch enclosure case is 53.9 × 44.8 × 17 mm. The wristwatch strap is made of silicone rubber with a measured ϵ_r = 3 and $tan\delta$ = 0.0001 at 915 MHz. The wristwatch is placed on a commercial SPEAG SHO-GFPC-V1 arm phantom model [14] to enable accurate

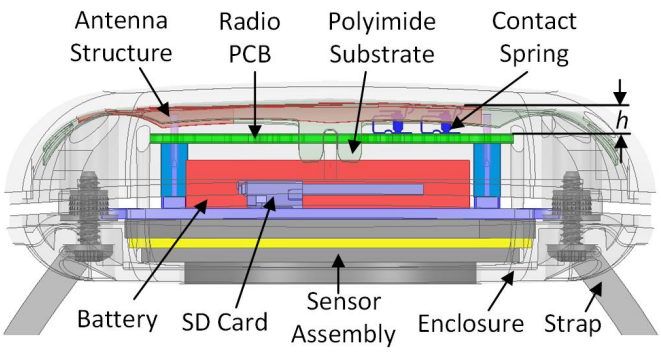

Fig. 3. Wristwatch model showing various internal components.

simulation of the antenna in the presence of the human wrist. The phantom model consists of an outer silicone material with ϵ_r = 30, electrical conductivity of σ = 0.7 S/m and a mass density of ρ = 1200 kg/m^3 at 915 MHz. The inner skeleton is has ϵ_r = 30 and σ = 2.5 S/m at 915 MHz [14]. As shown in Fig. 3, the wristwatch model includes all internal components that are present in the physical device as derived from CAD import of the mechanical design. All components such as the battery, radio printed circuit board (PCB), SD card, sensor assemblies were included to ensure accurate EM modelling of the entire assembly.

III. Antenna Simulations

This section presents a parametric study of several key antenna parameters that were used to optimize the performance of the antenna. This section also analyzes the surface current distribution and SAR performance of the antenna. The proposed antenna was simulated using Ansys full-wave high-frequency structure simulator (HFSS) [15].

A. Parametric Analysis

A parametric analysis was performed for L_1, L_2, W_3 and W_4 to study the effects of these parameters on the impedance characteristics of the antenna. It can be seen from Fig. 4(a) that parameter L_1 mainly controls the resonant frequency of the antenna when varied from 1 to 4 mm. This is explained by observing that resonator R_1 as shown in Fig. 1 has an estimated total length (measured along the centre) (L_{SA}) of 54 mm that corresponds to a guided electrical length of $0.28\lambda_g$ or close to $\lambda_g/4$ at 915 MHz. This calculation assumes the metal resonator is dielectrically loaded mainly by the ASA enclosure material (ϵ_r = 2.9) in direct contact with the copper interconnect for the antenna. Similarly, it can be seen in Fig. 4(b) that parameter L_2 determines the total length of the resonator R_2 and increasing the total length of R_2 causes a decrease in the resonant frequency. Also, in comparison to L_2, L_1 has more influence on the impedance matching of the antenna. Resonator R_2 is positioned further away from the radio board ground plane (see Fig. 1), whereas resonator R_1 is located closer to the radio board plane. Thus, in comparison to R_2, a lower mutual impedance between resonator R_1 and radio board ground plane is expected, and thus changing the

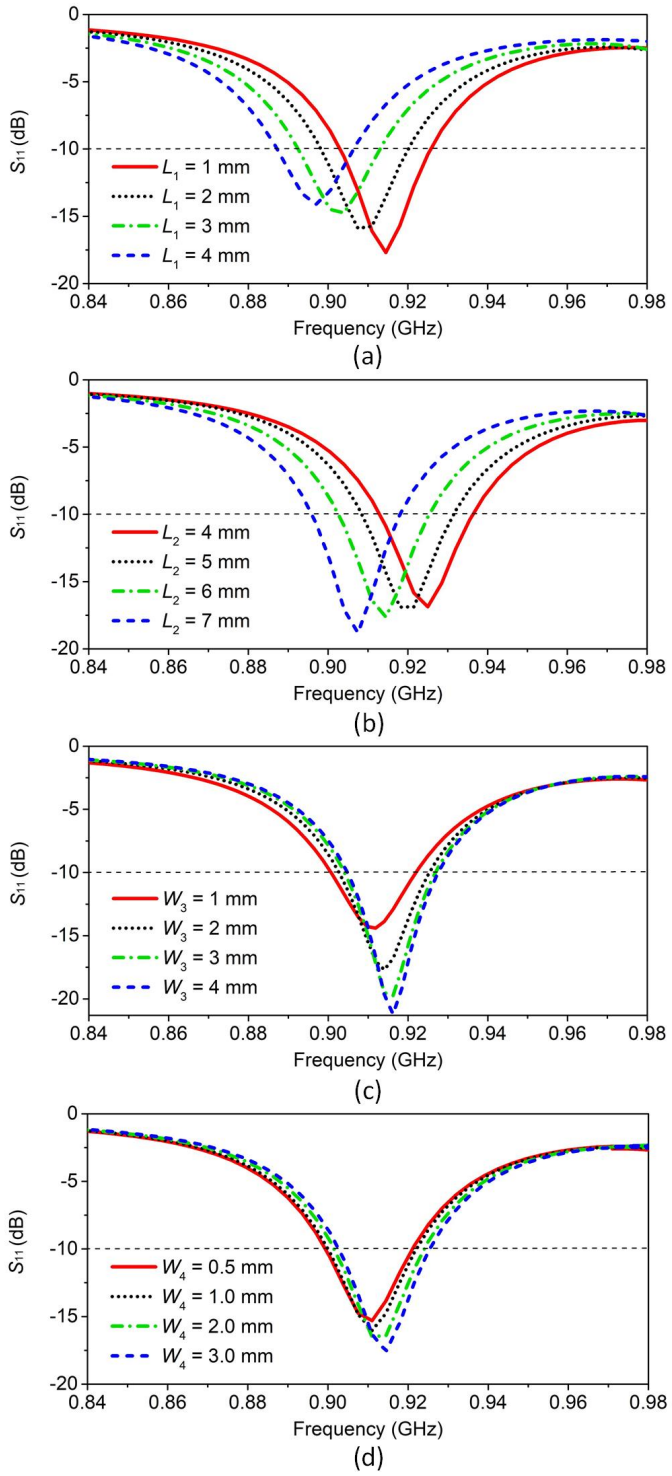

Fig. 4. Simulated S_{11} response for (a) varying L_1, (b) varying L_2, (c) varying W_3, and (d) varying W_4.

length R_1 has more effect on the input impedance of the antenna. Next, parameter W_3 was varied between 1 to 4 mm, and the resulting S_{11} response is shown in Fig. 4 (c). It is observed that increasing the width W_3, results in a small increase in resonant frequency and the parameter S_{11} improves significantly. This is expected since the inductive section between the signal and ground points at the antenna feed point is primarily used for impedance matching at the antenna feed point. Lastly, the parameter W_4 was varied between 0.5 mm to 3 mm, and the resulting S_{11} response is shown in Fig. 4 (d). Increasing the value of width W_4 results in a small resonant frequency increase, and the matching improves slightly having a similar behaviour to parameter W_3. The final optimized antenna parameters were chosen as $L_1 = 1$ mm, $L_2 = 6$ mm, $W_3 = 2$ mm and $W_4 = 3$ mm.

B. Surface Current and SAR Distribution

Fig. 5 (a and b), show the simulated surface current distribution on the antenna element and ground plane at 915 MHz. Large currents are observed on resonators R_1 and R_2 at 915 MHz. A large current is also observed at point *a* along the shunt inductive tuning path across the antenna feed between the signal and ground contacts. This is expected due to the low impedance (small resistive and inductive components) along this signal path. Large currents are also observed along paths *a* to *b* and *a* to *c*. Strong coupling exists between the antenna and motherboard and these paths represent the path of return current flow from the radio ground plane to the ground plane of the motherboard via the ground pin connections in connectors J_1 and J_2. Fig. 5(c) shows the simulated SAR distribution on a Speag phantom arm [14] at 915 MHz. For an input power of 1 mW, the peak SAR of 0.003 W/kg was achieved. This value is 3 orders of magnitude lower than the maximum permissible SAR value of 4 W/kg averaged over 10 grams of wrist tissue [16]. Fig. 5(d) shows a vector plot of E-field distribution between the antenna and wrist. It can be seen that E-field propagation (from point *p* to *q*) in a vertical direction is prevented via the two ground planes present in the radio and motherboard PCBs. However, since these ground planes are

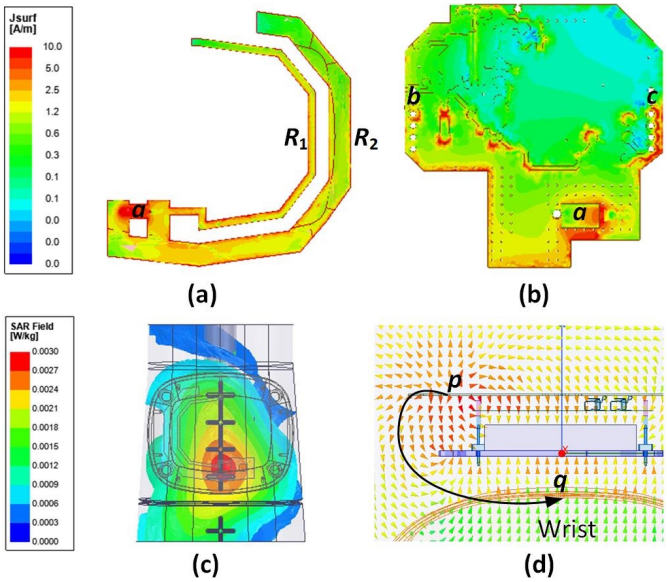

Fig. 5. At 915 MHz: (a) Surface current on antenna structure, (b) Surface current on ground plane, (c) SAR distribution, and (d) E-field distribution.

finite, E-field propagation is possible along the path *pq* shown, leading to peak SAR value beneath the antenna element.

IV. Antenna Measurements

In order to validate the simulated results, a prototype of the proposed antenna was fabricated and measured. In Fig. 6 the photographs of the wristwatch model, antenna and the internal components are illustrated. The measurements of the device under test (DUT) were taken after placing the wristwatch on the Speag phantom arm [14]. The antenna S_{11} was measured using a Rohde & Schwarz ZVRE vector network analyzer (VNA) [17]. Fig.7 shows the simulated and measured S_{11} responses that are in reasonable good agreement. The measured bandwidth is 30 MHz compared to 23 MHz for the simulated case. This is most likely attributed to additional losses in the measured case that are not accounted for in simulations. The radiation characteristics of the antenna were measured using an AMS-8050 antenna measurement system [18], as shown in Fig. 8. The simulated and measured radiation pattern of the antenna are shown in Fig. 9 and are seen to be in reasonable agreement. The antenna exhibits omni-directional radiation characteristics in the *xy*-plane as shown in 9 (a). The antenna also exhibits nulls in the *yz* and *xz*-planes. These nulls are expected due to the shielding effect of the finite PIFA ground plane in combination with body absorption of energy in the axis normal to the PIFA ground plane. The antenna (on-body) has a measured peak realized gain of -4.9 dBi and a radiation efficiency of 15.9% at 915 MHz, compared to -5.1 dBi and 19.8% respectively, for the simulated case. In order to assess the performance of the proposed antenna, a comparison against several state-of-the-art Sub-GHz band wrist-worn antennas was conducted and is summarized in Table I.

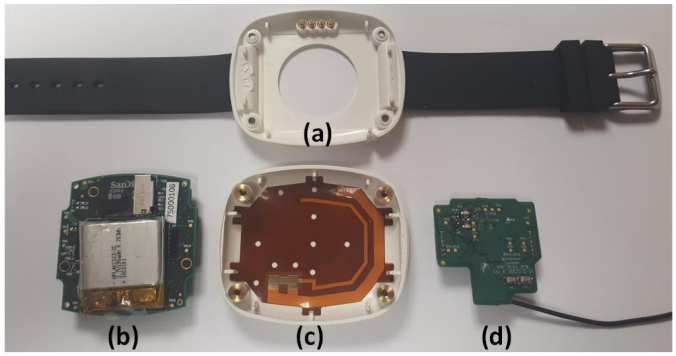

Fig. 6. Wristwatch model assembly: (a) Wristwatch enclosure, (b) Sensor assembly with battery, (c) Antenna prototype, and (d) Radio PCB.

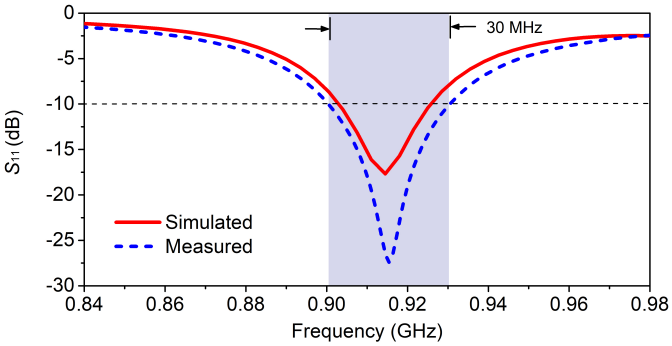

Fig. 7. Simulated versus measured S_{11} response of the antenna.

It can be observed that the majority of the antennas listed in Table I do not have simultaneously good impedance and radiation characteristics in contrast to the proposed antenna. In addition, all of the reported antennas except for [4], assume an ideal environment close to the antenna element and do not take

TABLE I
Comparison of State-of-the-Art Sub-GHz Band Wrist-Worn Antennas

Ref.	Antenna Dimensions (mm) $l \times w \times h^*$	Total Volume (mm^3)	Resonant Frequency, f_0 (MHz)	Peak Realized Gain at f_0 (dBi)	-10 dB Impedance Bandwidth (MHz)	Peak Radiation Efficiency at f_0(%)	Average SAR (W/kg)	Matching Network (Yes/No)
[4]	$44 \times 28 \times 1.6$	1971	915	-6.09	55	NA	NA	Yes
[5]	$40 \times 30 \times 10$	12000	920	NA	180	6.4	NA	No
[6]	$145 \times 40 \times 1.6$	9280	900	NA	160	6.3	0.18	No
[7]	$110 \times 29 \times 1.55$	4944	868	-13	17	NA	NA	No
[8]	$43.5 \times 28.5 \times 10.3$	12769	915	-0.57	26.4	46.8	0.004	No
[9]	$86 \times 25 \times 1.6$	3440	915	-6.87	19	NA	NA	No
[10]	$226 \times 30 \times 6$	40680	880	NA	30	83.7	NA	No
[11]	$50 \times 35 \times 3$	5250	868	-1.44	3.5	NA	0.0002	Yes
This work	**$48 \times 41 \times 2.3$**	**4526**	**915**	**-4.9**	**30**	**15.9**	**0.003**	**No**

* Antenna height (h) is measured from the nearest ground plane as illustrated in Fig. 3.

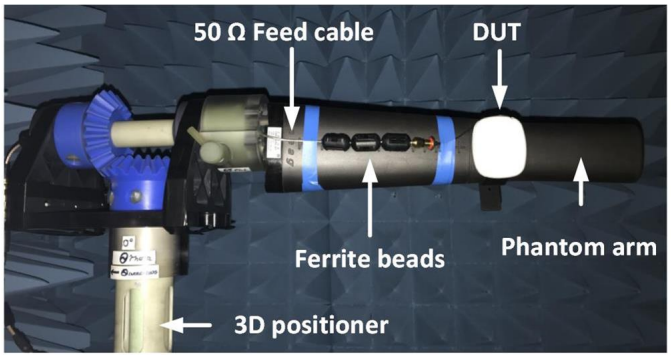

Fig. 8. DUT measurement setup in AMS-8050 anechoic chamber [18].

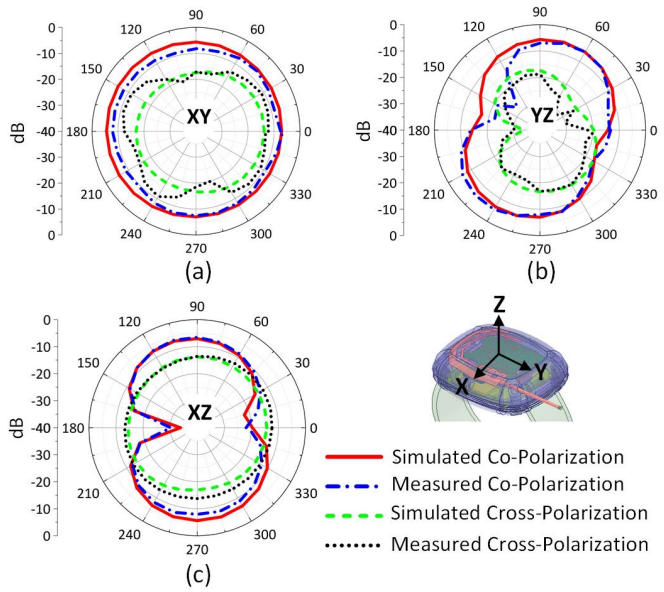

Fig. 9. Simulated and measured radiation characteristics of the antenna at 915 MHz (a) *xy*-plane, (b) *yz*-plane, and (c) *xz*-plane.

into account the effects of nearby internal components within a practical wireless device (e.g. internal components and assemblies such as PCBs, battery, connectors, metal screws, plastic components etc). In contrast, all of these components have been carefully modelled in this work.

V. Conclusion

This paper has presented a compact 915 MHz wristwatch planar inverted-F antenna. The proposed wristwatch-integrated antenna was simulated, manufactured, and characterized. Good agreement between simulated and measured results has been demonstrated. The measured on-body prototype antenna has a -10 dB impedance bandwidth of 30 MHz meeting the minimum bandwidth requirements of 26 MHz for the 915 MHz band operation. The measured on-body results show an on-body peak realized gain of -4.9 dBi and a peak radiation efficiency of 15.9% at 915 MHz. Moreover, for an input power of 1 mW, the simulated SAR of 0.003 W/kg, averaged over 10 grams of wrist tissue has been achieved, or three orders of magnitude less than the SAR limits. The measured antenna results have simultaneously good impedance and radiation performance and compares well with the state-of-the-art Sub-GHz band wrist-worn antennas.

Acknowledgment

We would like to acknowledge the support of Enterprise Ireland and the IDA for funding Innovation Partnership Project No IP20170559. We also acknowledge support from Science Foundation Ireland under grant 13/RC/2077 (CONNECT) as well as the support of Andrew Wallace and team from National Instruments for their continued support with the AWR toolset. This project is co-funded by the European Regional Development Fund (ERDF) under Ireland's European Structural and Investment Funds Programmes 2014-2020.

References

[1] P. Sundaravadivel, E. Kougianos, S. P. Mohanty and M. K. Ganapathiraju, "Everything you wanted to know about smart health care," *IEEE Consumer Electronics Mag.*, vol. 7, no. 1, pp. 18-28, Jan. 2018.

[2] D. Wu and S. W. Cheung, "A cavity-backed annular slot antenna with high efficiency for smartwatches with metallic housing," *IEEE Trans. Antennas Propag.*, vol. 65, no. 7, pp. 3756-3761, May 2017.

[3] R. Cavallari, F. Martelli, R. Rosini, C. Buratti and R. Verdone,"A Survey on wireless body area networks: Technologies and design challenges,"*IEEE Commun. Surveys & Tutorials*, vol. 16, no. 3, pp. 1635-1657, Feb. 2014.

[4] A. D. Serio *et al.*, "Potential of Sub-GHz wireless for future IoT wearables and design of compact 915 MHz antenna," *Sensors*, vol. 18, no. 1, Dec. 2017.

[5] C. Hong and S. Yeh, "Cellular antenna design with metallic housing for wearable device," *Asia-Pacific Conf. on Antennas and Propag.*, pp. 419-420, July 2016.

[6] K. Zhao, Z. Ying, and S. He, "Antenna designs of smart watch for cellular communications by using metal belt," *European Conf. on Antennas and Propag.*, pp. 1-5, Aug. 2015.

[7] S. Lopez-Soriano and J. Parron, "Design of a Small-Size, low-profile and low-cost normal-mode helical antenna for UHF RFID wristbands," *IEEE Antennas Wireless Propag. Lett.*, vol. 16, pp. 2074-2077, April 2017.

[8] S. Kumar *et al.* ,"A Bandwidth Enhanced 915 MHz Antenna for IoT Wrist-Watch Applications,"*European Conf. on Antennas and Propag.*, Krakow, Poland, pp. 1-5, April 2019.

[9] Guan-Long Huang, Chow-Yen-Desmond Sim, Shu-Yao Liang, Wei-Sheng Liao, and Tao Yuan,"Low-profile flexible UHF RFID tag design for wristbands applications,"*Wireless Commun. and Mobile Computing*, 13 pages, vol. 2018, June. 2018.

[10] X. Gao *et al.*, "A novel wrist wear dual-band diversity antenna,"*IEEE Antennas and Propag. Society Int. Symp.*, pp. 1-4, July 2009.

[11] M. Feliziani and F. Maradei,"Antenna design of a UHF RFID tag for human tracking avoiding spurious emission,"*IEEE Int. Symp. on Electromagnetic Compatibility*, pp. 245-248, Pittsburgh, PA, Aug. 2012.

[12] K. Eroglu, "The worldwide approval status for 900 MHz and 2.4 GHz spread spectrum radio products," *Int. Symp. on Electromagnetic Compatibility*, vol. 2, pp. 1131-1135, Aug. 1998.

[13] Speag Dielectric Assessment Kit: DAK3.5-TL, Available online: https://speag.swiss/products/dak/dak-dielectric-probe-systems/dak3-5tl-p-200mhz-20ghz/, Accessed in Oct. 2019.

[14] Speag phantom arm: SHO-GFPC-V1, Available online: https://speag.swiss/products/em-phantoms/phantoms/sho-gfpc-v1/, Accessed in Oct. 2018.

[15] ANSYS HFSS, Available online: http://www.ansys.com/products/electronics/ansys-hfss, Accessed in Oct. 2019.

[16] P. Bernardi, M. Cavagnaro, S. Pisa and E. Piuzzi,"Specific absorption rate and temperature elevation in a subject exposed in the far-field of radio-frequency sources operating in the 10-900-MHz range,"*IEEE Trans. Biomed. Eng.*, vol. 50, no. 3, pp. 295-304, Mar. 2003.

[17] Rohde & Schwarz ZVRE vector network analyzer, Available online: *https://www.rohde-schwarz.com*, Accessed in Oct. 2019.

[18] ETS-LINDGREN: AMS-8050 antenna measurement system, Available online: *http://www.ets-lindgren.com/*, Accessed in Oct. 2019.